Sensors & Transducers, Vol. 226, Issue 10, October 2018, pp. 100-106

Sensors & Transducers
Published by IFSA Publishing, S. L., 2018
http://www.sensorsportal.com

Light Rays Scattered by Homogeneous and Coated Cones Based on Vectorial Complex Rays Model

[1, 2] Qingwei DUAN, [1] Xiang'e HAN and [2] Kuan Fang REN
[1] School of Physics and Optoelectronic Engineering, Xidian University, Xi'an, 710071, China
[2] CORIA-UMR 6614, Normandie Université, CNRS, Université et INSA de Rouen, 76801 Saint Etienne du Rouvray, France
[2] Tel.: +(33)0232953743, fax: +(33)0232953794
[2] E-mail: fang.ren@coria.f

Received: 25 June 2018 /Accepted: 31 August 2018 /Published: 31 October 2018

Abstract: The light scattering of objects is essential for its wide applications in optical measurement for the merit of convenience and no-intervention. Although many theories, models and numerical algorithms have been developed, the light scattering by large non-spherical objects is still a bottleneck problem in this field. In the Vectorial Complex Ray Model (VCRM) we have developed, the wavefront curvature is introduced as a new intrinsic property of rays. Due to this new conception, VCRM is shown much convenient and precise to predict the light scattering by large non-spherical objects. In this paper, we will present an application of VCRM in the light scattering by homogeneous and coated cones. The analysis of the scattering properties calculated by our code is also given. We found that for the homogeneous cone, the position of rainbow is very sensitive to the cone slope, and for the coated cone, the angle difference between the twin rainbows is highly sensitive to the coating thickness. This work is hoped to provide new ideas for real-time and non-intrusive measurement of liquid jets and tapered fibers.

Keywords: Light scattering, Homogeneous cone, Coated cone, Vectorial Complex Ray Model, Rainbow, Liquid jet, Tapered fiber.

1. Introduction

Optical measurement techniques are being applied in many fields to obtain information about the scatterers due to their advantages of being non-intrusive, rapid and reliable. The theories and models to describe the relation between the scattered light and the different kinds of particles are essential.

However, most optical techniques are limited to spherical particles or very small objects because of the lack of theories and models for large non-spherical objects. For examples, liquid jets breakup [1-2] is essential for atomization process whereas the cross section of a liquid jet, even in the simplest configuration, varies with the distance from the exit; furthermore, the tapered fibers [3-4] have recently attracted considerable interest for a wide variety of photonic applications [5-6], and those types of fibers have linearly varying cross sections. To develop relevant optical measurement technique, we must be able to predict the scattering of such kinds of objects.

In Vectorial Complex Ray Model (VCRM) [7-8] we developed in recent years, the wavefront curvature is introduced as an intrinsic property of rays. This new conception improves considerably the precision of classical ray models. Moreover, by vectorizing the light rays, the calculation for the directions of scattering rays is considerably simplified, especially in

the cases of 3D non-spherical objects [9-10]. In this paper, we will apply VCRM to the study on the light scattering of homogeneous and coated cones.

The outline of this paper is as follows: Section 2 describes the models of homogeneous and coated cones. In Section 3, the ray tracing method for 3D objects is introduced. Section 4 shows the simulation results and discusses the scattering characteristics of homogeneous and coated cones. Section 5 summarizes our results.

2. Mathematical Models of Homogeneous and Coated Cones

The schematic diagrams of homogeneous and coated cones are shown in Fig. 1. The transversal radius of the homogeneous cone r is a linear function of z:

$$r(z) = a + bz\,, \tag{1}$$

where a is the initial radius at $z=0$, and b is the slope along the cone axis. The homogeneous cone has a refractive index of n_2, and its surroundings are of n_1.

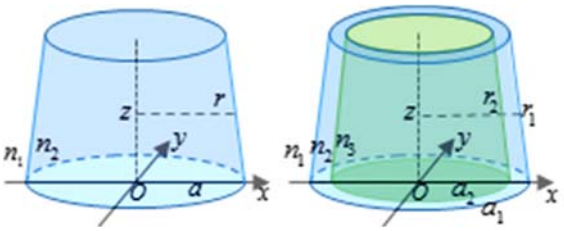


Fig. 1. Schematic diagrams of homogeneous and coated cones.

While for the coated cone, two functions are needed to describe its internal and external surfaces.

$$\begin{aligned} &\text{For external surface:} \quad r_1(z) = a_1 + b_1 z \\ &\text{For internal surface:} \quad r_2(z) = a_2 + b_2 z \end{aligned} \tag{2}$$

The inside medium is usually referred to as the core, while the coated medium is refered to as the coating. The refractive indices of the surroundings, coating and the core are n_1, n_2 and n_3, respectively. Besides, the thickness of the coating Δr at a position z is defined as $r_1(z) - r_2(z)$.

Each of the surface functions in Eqs. (1) and (2) can be written in the implicit form $F(x,y,z)=0$. The unit vector normal to this surface at an arbitrary point can be obtained by calculating the gradient:

$$\hat{n} = \left(F_x, F_y, F_z\right) \Big/ \sqrt{F_x^2 + F_y^2 + F_z^2}\,, \tag{3}$$

where F_x, F_y and F_z represent the partial differentials $\partial F/\partial x$, $\partial F/\partial y$ and $\partial F/\partial z$, respectively.

3. Ray Tracing Method for 3D Scattering

In VCRM, the directions of light rays are represented by their wave vectors, and a local coordinate system is established at the point of interaction. This can considerably simplify the computation for the directions of refracted and reflected waves. When a light ray $\boldsymbol{k}^i$ is incident on the surface of a 3D object, the plane of incidence Σ_{inc} is defined by the incident wave vector $\boldsymbol{k}^i$ and the normal vector $\hat{n}$. Here we introduce an auxiliary vector $\hat{v}$ as:

$$\hat{v} = \boldsymbol{k}^i \times \hat{n} \Big/ \left\| \boldsymbol{k}^i \times \hat{n} \right\| \tag{4}$$

Then the unit vector $\hat{\tau}$ tangent to the object surface and located in Σ_{inc} is obtained by:

$$\hat{\tau} = \hat{v} \times \hat{n} \tag{5}$$

The relation between these quantities are illustrated in the Fig. 2.

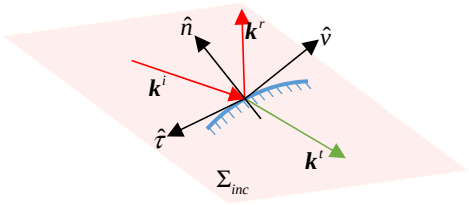


Fig. 2. Local coordinate system $(\hat{n},\hat{\tau},\hat{v})$ at the surface of a 3D object is introduced to describe the incident wave vectors $\boldsymbol{k}^i$, the reflected $\boldsymbol{k}^r$ and the refracted $\boldsymbol{k}^t$.

The normal and tangent components of the incident wave vector $\boldsymbol{k}^i$ can be evaluated by $k_n^i = \boldsymbol{k}^i \cdot \hat{n}$ and $k_\tau^i = \boldsymbol{k}^i \cdot \hat{\tau}$, respectively. According to the Snell law that the tangent component of the wave vector is continuous at the boundary, i.e. the tangent components of the wave vectors of the incident wave, the reflected wave and the refracted wave are identical:

$$k_\tau^i = k_\tau^r = k_\tau^t \tag{6}$$

The normal components are calculated by

$$\begin{cases} k_n^r = -k_n^i & \text{reflected wave} \\ k_n^t = \sqrt{k_t^2 - k_\tau^{i2}} & \text{refracted wave} \end{cases}, \tag{7}$$

where k_t is the wave number of the refracted wave. If total reflection occurs, there is no refracted ray in the framework of ray optics.

Then, the refracted wave vector $\boldsymbol{k}^t$ in the local coordinate bases $(\hat{n},\hat{\tau},\hat{v})$ is obtained as $\boldsymbol{k}^t = k_n^t\hat{n} + k_\tau^t\hat{\tau}$, and its expression in the global coordinate bases $(\hat{x},\hat{y},\hat{z})$ is acquired by:

$$\begin{bmatrix} k_x^t \\ k_y^t \\ k_z^t \end{bmatrix} = \begin{bmatrix} k_n^t n_x + k_\tau^t \tau_x \\ k_n^t n_y + k_\tau^t \tau_y \\ k_n^t n_z + k_\tau^t \tau_z \end{bmatrix} \tag{8}$$

The reflected wave vector $\boldsymbol{k}^r$ can be calculated in a similar way.

Besides, to describe the directions in 3D space, the azimuth angle φ and the elevation angle ψ are used. The former is the angle made with the *XOZ* plane (the incident rays are along the *x*-axis), and its value $\varphi = \text{atan2}(k_y,\ k_x)$; while the latter depicts how much a ray is elevated from the horizontal plane, and it is evaluated as $\psi = \arctan\left(k_z \Big/ \sqrt{k_x^{\,2} + k_y^{\,2}}\right)$.

Another problem in ray tracing is to find the coordinates of the next interaction point. Here we introduce the distance factor t, then the ray between two successive interaction points in a homogeneous medium can be expressed as:

$$\begin{aligned} x &= x_N + t \cdot k_x \\ y &= y_N + t \cdot k_y \\ z &= z_N + t \cdot k_z \end{aligned}, \tag{9}$$

where (k_x, k_y, k_z) is the wave vector which originates from the interaction point (x_N, y_N, z_N). Then the coordinates of next interaction point can be solved by substituting Eq. (9) into the surface function, i.e.

$$F\left(x_N + t\cdot k_x, y_N + t\cdot k_y, z_N + t\cdot k_z\right) = 0 \tag{10}$$

This is an equation with one variable. Then the problem of seeking the next point of interaction is now boiled down to solving this equation [9].

In the specific case of a homogeneous cone with a radius of $r(z) = a + bz$, the current point (x_N, y_N, z_N) and the next point of interaction $(x_{N+1}, y_{N+1}, z_{N+1})$ satisfy the same surface function, so we have

$$\begin{cases} x_N^{\,2} + y_N^{\,2} = (a + bz_N)^2 \\ (x_N + tk_x)^2 + (y_N + tk_y)^2 = \left[a + b(z_N + tk_z)\right]^2 \end{cases} \tag{11}$$

from which we can deduce the distance factor t for a homogeneous cone (the solution $t = 0$ corresponds to the current point and should be omitted):

$$t = \frac{2\left(abk_z + b^2 k_z z_N - k_x x_N - k_y y_N\right)}{k_x^{\,2} + k_y^{\,2} - b^2 k_z^{\,2}} \tag{12}$$

While for a coated cone, it becomes a little complicated. Let's suppose the current point is on the cone of $r_i(z) = a_i + b_i z$, while the next point is on the cone of $r_j(z) = a_j + b_j z$, where *i* and *j* are equal to either 1 or 2 but $i \neq j$ if the two points are on different surfaces. They satisfy

$$\begin{cases} x_N^{\,2} + y_N^{\,2} = (a_i + b_i z_N)^2 \\ (x_N + tk_x)^2 + (y_N + tk_y)^2 = \left[a_j + b_j(z_N + tk_z)\right]^2 \end{cases} \tag{13}$$

This set of equations can be reduced as

$$At^2 + Bt + C = 0, \tag{14}$$

where the coefficients *A*, *B* and *C* are defined as

$$\begin{aligned} A &= \left(k_x^{\,2} + k_y^{\,2} - b_j^{\,2} k_z^{\,2}\right) \\ B &= 2\left[k_x x_N + k_y y_N - \left(a_j + b_j z_N\right) b_j k_z\right] \\ C &= (a_i + b_i z_N)^2 - (a_j + b_j z_N)^2 \end{aligned} \tag{15}$$

Then, the solution to the variable t is obtained as $t_1,\ t_2 = \left(-B \pm \sqrt{B^2 - 4AC}\right) \Big/ 2A$. Actually, in the case when the two successive points are on the same cone, i.e. $a_i = a_j$ and $b_i = b_j$, the coefficient C is equal to 0, and this leads to $t = -B/A$ which coincides with the solution for a single homogeneous cone (see Eq. (12)). In another case, if the next point of interaction is on the surface of another cone, i.e. $a_i \neq a_j$ and $b_i \neq b_j$, the two solutions t_1 and t_2 correspond to two intersection points, and we need to judge which one maps the actual point of interaction: if t_1 and t_2 are of different signs, the right answer to t is the positive one; if both of them are positive, the smaller one is the right answer. In the end, by substituting the obtained value of t into Eq. (9), the coordinates of the next point of interaction are acquired.

Through the procedure introduced above, the directions and the exit positions of all scattering rays can be calculated. In the following section, the simulation results for the light rays scattered by homogeneous and coated cones are presented.

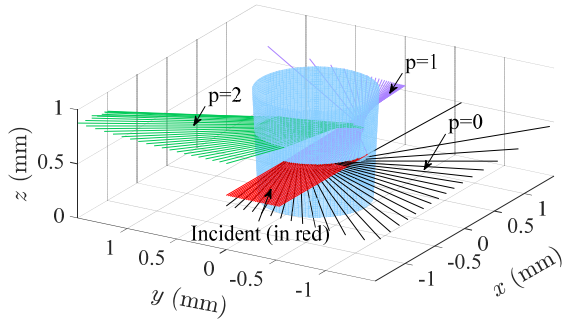
4. Results

In this work, plane wave of incidence is concerned. And in the framework of ray optics, the plane wave can be simulated as the aggregation of vast discrete rays which are parallel to each other [11-13].

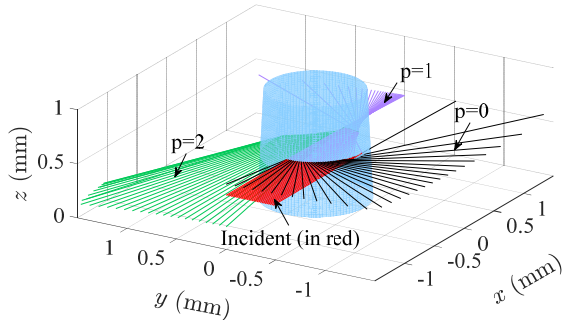
4.1. Light Rays Scattered by Homogeneous Cones

The homogeneous cone used in simulation has an initial cross section of $r(0)=a=0.5$ mm and a variable slope b. The wavelength of the incident light $\lambda=632.8$ nm, the refractive indices $n_1=1$ and $n_2=1.333$. The simulation result is shown in Fig. 3.

The z value of the plane where the incident rays are located is 0.5 mm, and p is the order of the scattering rays (following the convention, the scattering rays of p order have undergone $p+1$ times of interaction with the particle). We can see from Fig. 3 that the scattering rays of different p orders are no longer in the same plane, which means the interference at infinity (or on a focal plane of a collection lens) only happens between the rays with the same p. That is very different from the scattering of a circular cylinder.



(a) $b=0.05$ (radius expands with z)



(b) $b=-0.05$ (radius contracts with z)

Fig. 3. Tracing of the light rays scattered by an expanding cone and a contracting cone. For clarity, only the scattering rays of $p \le 2$ are drawn.

However, as shown in Fig. 4, the scattering rays of $p \ge 2$ may still concentrate at the extremal angle of their own. We define the density of the scattering rays as the percentage of the number of the rays arriving at an interval of 1°, i.e.

$$\eta = \frac{\text{number of rays in } 1^\circ}{\text{total number of rays}} \times 100\% \qquad (16)$$

Moreover, to mark the incident positions of different incident rays, a quantity ζ called impact factor is used. The incident ray which impacts the cone axis has an impact factor $\zeta=0$; while $\zeta=1$ indicates the ray of grazing incidence.

For example, as shown in Fig. 4, the density η of the $p=2$ rays shows a distinct peak around 138°, at which the azimuth angle φ (varies with ζ) reaches a minimum value. These angles for $p=2, 3, 4, \ldots$ define respectively the horizontal positions of the 1st, 2nd, 3rd ... rainbows [14-15].

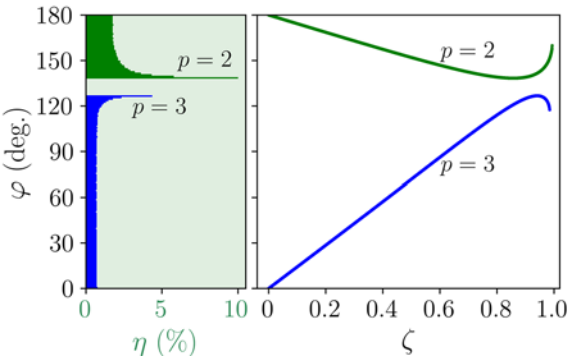


Fig. 4. The azimuth angle distribution of the $p=2$ and $p=3$ rays. The parameters are the same as in Fig. 3(b).

It was found that the angular positions of the rainbows, especially the elevation angles, are very sensitive to the slope of cone. By changing the value of the slope, the corresponding spatial positions of the 1st rainbows are calculated and are given in Fig. 5.

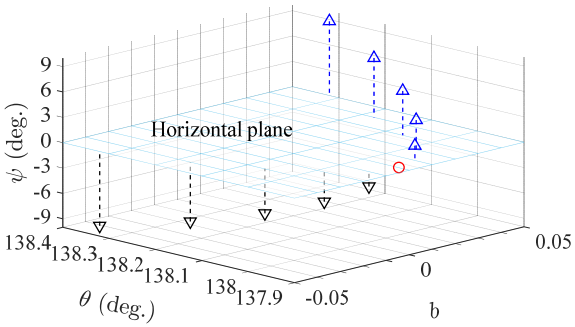


Fig. 5. Variation of the spatial position (φ,ψ) of the 1st rainbow with the cone's slope b.

We can see that as the slope b varies from -0.05 to 0.05 (the homogeneous cone is changed from slightly contracting to slightly expanding), the elevation angle ψ of the 1st rainbow is altered from -8.8° to $+8.8^\circ$, while the azimuth angle φ varies in range of $[137.9^\circ, 138.3^\circ]$. When $b=0$, the homogeneous cone degenerates into an infinite cylinder with all scattering rays located in the horizontal plane. This explains why the elevation angle equals 0 in this case.

4.2. Light Rays Scattered by Coated Cones

For a coated cone, we are concerned about the scattering rays that have been internally reflected once respectively by the core and the coating (the classes α and β rays shown in Fig. 6). This setup is chosen because these light rays permit to study relatively easily the formation of the twin rainbows [16-19].

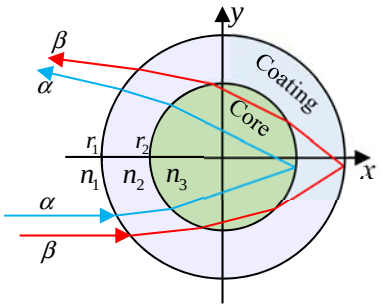


Fig. 6. Top view of the paths of the α and β rays.

In [17], the authors studied on the twin rainbows of coated cylinders and found that the angle differences between the two rainbows are tightly related to the thickness of coating. In this paper, we will study the light rays scattered by a coated cone whose inner and outer radii vary linearly. It is more complicated but is of same importance.

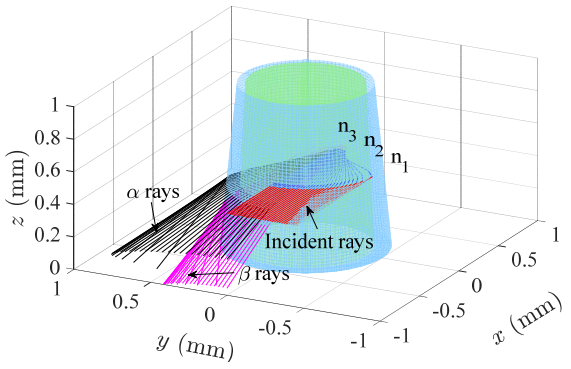
In the case of $n_1 < n_2 > n_3$, for example the air-water-air model, there is no extremal angle for the scattering rays of class α or β, then twin rainbows do not exist. When the refractive index model is of $n_1 < n_2 < n_3$, the twin rainbows can be formed. Here we note the rainbow formed by those class α rays as the α rainbow, and that by the β rays as the β rainbow.

The coated cone in our simulation is composed of two concentric circular cones, and the two cones are of different slopes: the external and internal surfaces are set as $r_1 = 0.5 - 0.10z$ and $r_2 = 0.4 - 0.05z$ mm, respectively; and the air-water-glass model ($n_1 = 1$, $n_2 = 1.333$ and $n_3 = 1.615$) is applied. The tracing result for the α and β rays is given in Fig. 7.

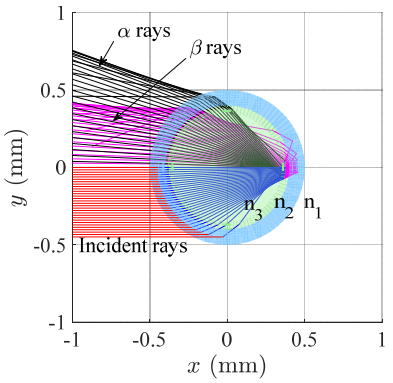
In Fig. 7, the z value of the plane where incident rays are located, noted as z_i in the following part, is 0.5 mm.

We can see that the α rays and β rays have their own extremal angles. The extremal value of the azimuth angles and the corresponding elevation angle define the spatial position of rainbow. In the following part, we will analyze how the positions of the α and β rainbows are distributed as z_i changes.

By moving the plane of incident rays from $z_i = 0.5$ mm to $z_i = 1.5$ mm, the azimuth angles φ and the elevation angles ψ of the twin rainbows are calculated (See the Table 1 and Fig. 8). We can see from the Table 1 and Fig. 8 that, as z_i changes from 0.5 mm to 1.5 mm, the azimuth angle φ of the a rainbow is increased by 4.8° , while the β rainbow is decreased by 2.8°; the elevation angles are almost unchanged because they are mainly determined by the slopes of the coated cone.



(a) Side view



(b) Top view

Fig. 7. Tracing of the light rays scattered by the coated cone. The classes α and β are the light rays that contribute to the twin rainbows.

Table 1. Variation of the α and β rainbows with z_i.

Z_i, mm	0.5	0.7	0.9	1.1	1.3	1.5
(r_1-r_2), μm	75	65	55	45	35	25
φ deg. (α)	159.26	160.13	161.04	162.00	163.01	164.08
φ deg. (β)	173.28	172.81	172.30	171.73	171.11	170.43
ψ deg. (α)	-14.99	-15.02	-15.05	-15.08	-15.10	-15.13
ψ deg. (β)	-22.53	-22.50	-22.47	-22.43	-22.39	-22.34

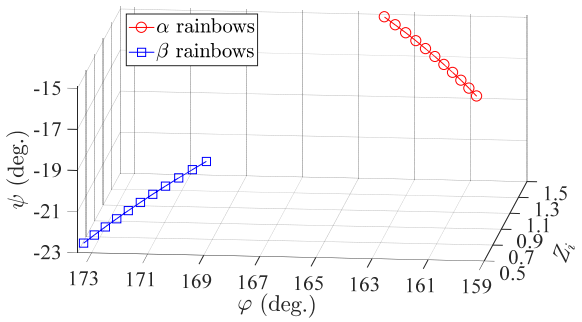


Fig. 8. Spatial positions of the α and β rainbows as z_i changes (plotting of the data in Table. 1).

Despite the constant slopes of inner and outer surfaces, the thickness $r_1 - r_2$ are shrunken from 75 μm to 25 μm, which is the cause why the azimuth angles are shifted.

It concludes that in the case of a coated cone, the elevation angles of twin rainbows are mainly determined by the slopes of the inner and outer cone surfaces; while the azimuth angles are tightly related to the thickness of coating. This sensitivity presents a promising way to measure the thickness of the coated cone by the angle distribution of the twin rainbows.

5. Conclusions

The ray tracing method based on VCRM is discussed in detail. By the ray tracing method, the light rays scattered by homogeneous and coated cones are simulated, and the analysis of the scattering properties are given in the framework of geometrical optics. It was found that the spatial positions of the rainbows by a homogeneous cone are very sensitive to the cone slope; and for a coated cone, the elevation angles of the twin rainbows are mainly determined by the inner and outer slopes, while the difference in the azimuth angles of the twin rainbows is tightly related to the thickness of coating. A full calculation for the amplitude and the phase with VCRM is being undertaken. This work is hoped to explore and understand the physical mechanism of light scattering by 3D irregular objects, and to provide new ideas to carry out non-intrusive measurement for liquid jets of circular or annular cross section, and the tapered fibers.

Acknowledgements

This work was funded by the Natural Science Basic Research Plan in Shaanxi Province of China under Grant nos.2015KW-025, the China Scholarship Council, and the French National Research Agency, France, under the grant ANR-13-BS090008-01 (AMO-COPS). This work was also supported by the 111 Project under Grant B17035, China.

References

[1]. C. Clanet, J. C. Lasheras, Transition from dripping to jetting, *Journal of Fluid Mechanics*, Vol. 383, 1999, pp. 307-326.

[2]. N. Moallemi, R. Li, K. Mehravaran, Breakup of capillary jets with different disturbances, *Physics of Fluids*, Vol. 28, Issue 1, 2016, pp. 012101.

[3]. J. Villatoro, D. Monzón-Hernández, E. Mejía, Fabrication and modeling of uniform-waist single-mode tapered optical fiber sensors, *Applied Optics*, Vol. 42, Issue 13, 2003, pp. 2278–2283.

[4]. S. W. Harun, K. S. Lim, C. K. Tio, K. Dimyati, H. Ahmad, Theoretical analysis and fabrication of tapered fiber, *Optik*, Vol. 124, Issue 6, 2013, pp. 538-543.

[5]. Y. Tai, P. Wei, Sensitive liquid refractive index sensors using tapered optical fiber tips, *Optics Letters*, Vol. 35, Issue 7, 2010, pp. 944-946.

[6]. Z. Liu, C. Guo, J. Yang, L. Yuan, Tapered fiber optical tweezers for microscopic particle trapping: fabrication and application, *Optics Express*, Vol. 14, Issue 25, 2006, pp. 12510-12516.

[7]. K. F. Ren, F. Onofri, C. Rozé, T. Girasole, Vectorial complex ray model and application to two-dimensional scattering of plane wave by a spheroidal particle, *Optics Letters*, Vol. 36, Issue 3, 2011, pp. 370–372.

[8]. K. F. Ren, C. Rozé, Vectorial Complex Ray Model for light scattering of nonspherical particles, Chapter 7 in *Advances in Optics: Reviews, Book Series*, Vol. 1, IFSA Publishing, S. L, 2018.

[9]. Q. Duan, R. Zhong, X. Han, K. F. Ren, Influence of spatial curvature of a liquid jet on the rainbow positions: Ray tracing and experimental study, *Journal of Quantitative Spectroscopy and Radiative Transfer*, Vol. 195, 2017, pp. 156-163.

[10]. Q. Duan, K. F. Ren, X. Han, Simulation of the light rays scattered by homogeneous and coated cones based on vectorial complex rays model, in *Proceedings of the 1st International Conference on Optics, Photonics and Lasers (OPAL'18)*, Barcelona, Spain, 9-11 May 2018, pp. 131-135.

[11]. H. He, W. Li, X. Zhang, M. Xia, K. Yang, Light scattering by a spheroidal bubble with geometrical optics approximation, *Journal of Quantitative Spectroscopy and Radiative Transfer*, Vol. 113, Issue 12, 2012, pp. 1467-1475.

[12]. H. Yu, J. Shen, C. Tropea, Application of vector ray tracing to the computation of Möbius shifts for the primary and secondary rainbows, *Applied Optics*, Vol. 54, Issue 31, 2015, pp. 9093-9101.

[13]. H. Yu, J. Shen, Y. Wei, Geometrical optics approximation of light scattering by large air bubbles, *Particuology*, Vol. 6, Issue 5, 2008, pp. 340-346.

[14]. Van de Hulst H. C., Light scattering by small particles, *Dover Publications*, 1981.

[15]. J. A. Adam, The mathematical physics of rainbows and glories, *Physics Reports*, Vol. 356, Issue 4-5, 2002, pp. 229-365.

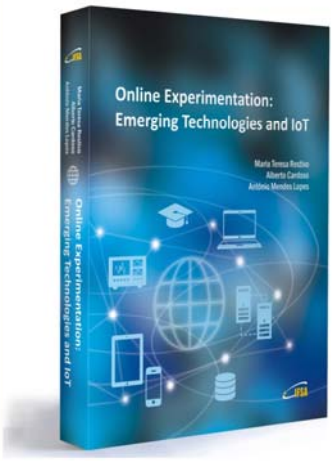
[16]. J. Lock, J. Jamison, C. Lin, Rainbow scattering by a coated sphere, *Applied Optics*, Vol. 33, Issue 21, 1994, pp. 4677-4690.

[17]. C. Adler, J. Lock, I. Rafferty, W. Hickok, Twin-rainbow metrology. I. Measurement of the thickness of a thin liquid film draining under gravity, *Applied Optics*, Vol. 42, Issue 33, 2003, pp. 6584-6594.

[18]. F. Song, C. Xu, S. Wang, Twin primary rainbows scattering by a liquid-filled capillary, *Optics Communications*, Vol. 332, 2014, pp. 96-102.
[19]. M. Zhai, Q. Lü, H. Zhang, Y. Zhang, Coated sphere scattering by geometric optics approximation, *Journal of the Optical Society of America A*, Vol. 31, Issue 10, 2014, pp. 2160-2169.

Published by International Frequency Sensor Association (IFSA) Publishing, S. L., 2018 (http://www.sensorsportal.com).

IFSA



Hardcover: ISBN 978-84-608-5977-2
e-Book: ISBN 978-84-608-6128-7

Online Experimentation: Emerging Technologies and IoT

Maria Teresa Restivo, Alberto Cardoso, António Mendes Lopes (Editors)

Online Experimentation: Emerging Technologies and IoT describes online experimentation, using fundamentally emergent technologies to build the resources and considering the context of IoT.

In this context, each online experimentation (OE) resource can be viewed as a "thing" in IoT, uniquely identifiable through its embedded computing system, and considered as an object to be sensed and controlled or remotely operated across the existing network infrastructure, allowing a more effective integration between the experiments and computer-based systems.

The various examples of OE can involve experiments of different type (remote, virtual or hybrid) but all are IoT devices connected to the Internet, sending information about the experiments (e.g. information sensed by connected sensors or cameras) over a network, to other devices or servers, or allowing remote actuation upon physical instruments or their virtual representations.

The contributions of this book show the effectiveness of the use of emergent technologies to develop and build a wide range of experiments and to make them available online, integrating the universe of the IoT, spreading its application in different academic and training contexts, offering an opportunity to break barriers and overcome differences in development all over the world.

Online Experimentation: Emerging Technologies and IoT is suitable for all who is involved in the development design and building of the domain of remote experiments.

Order: http://www.sensorsportal.com/HTML/BOOKSTORE/Online_Experimentation.htm